Journal of Power Sources 193 (2009) 160–164

Contents lists available at ScienceDirect

Journal of Power Sources

journal homepage: www.elsevier.com/locate/jpowsour

Short communication

Mitigation of carbon deposits formation in intermediate temperature solid oxide fuel cells fed with dry methane by anode doping with barium

D. La Rosa[a], A. Sin[b], M. Lo Faro[a], G. Monforte[a], V. Antonucci[a], A.S. Aricò[a,*]

[a] CNR-ITAE, Via Salita Santa Lucia Sopra Contesse 5, I-98125 Messina, Italy
[b] Pirelli Labs S.p.A., Viale Sarca 222, I-20126 Milan, Italy

ARTICLE INFO

Article history:
Received 7 October 2008
Received in revised form 26 January 2009
Accepted 27 January 2009
Available online 10 February 2009

Keywords:
IT-SOFCs
Ba-doping
Ni-Cu catalysts
Gadolinia doped ceria
Basicity
Direct utilization

ABSTRACT

The effect of barium doping on a fuel cell anode consisting of a $Ni_{0.53}Cu_{0.47}$ alloy and gadolinia doped ceria cermet (50:50 wt.) was investigated in an intermediate temperature solid oxide fuel cell (IT-SOFC) fed with dry methane. IT-SOFCs containing the same cathode-electrolyte configuration but equipped with different anodes were compared in terms of performance, steady state operation, and formation of carbon deposits on the anode surface. After proper cell conditioning, similar maximum power densities of 284 mW cm^{-2} and 310 mW cm^{-2} were obtained in dry methane fuel at 750 °C for the anodic compositions with and without barium, respectively. The anode containing barium did not show significant carbon deposits after a 200 h time-study in dry methane whereas the anode without barium showed the presence of carbon deposits as evidenced by X-ray diffraction (XRD). Both anode formulations showed carbon deposits when exposed to dry CH_4 in ex-situ experiments. The electrochemical profile recorded during the time-study was different in the two systems. In the absence of barium, a slow and progressive increase in performance as a function of time was achieved. On the contrary, the Ba-doped anode achieved optimum performance in a short time. It is determined that the presence of barium reduces carbon deposition under fuel cell conditions and influences the electrochemical behaviour.

1. Introduction

The direct utilization of dry hydrocarbons in solid oxide fuel cells is a promising process in terms of high efficiency and system simplicity. Various anode catalysts have been investigated for this process, including Cu and Ni-based cermets (e.g, Cu/CeO_2/YSZ, Ni-alloys, Cu-alloys) [1–8], various perovskites e.g. $(La_{0.75}Sr_{0.25})_{0.9}Cr_{0.5}Mn_{0.5}O_3$ [9], ceria based anodes doped with precious metals [10], Au/GDC [11], Cu–Co mixtures [12], niobium titanates [13], tungsten bronze [14], etc. The main drawback of this process is the carbon deposition that occurs, especially on Ni catalysts, leading to anode deactivation [15–17]. Preventing carbon deposition is, therefore, of primary importance for the use of Ni-based catalysts in direct oxidation processes. A reduction of carbon deposits was also observed in unmodified Ni catalysts at low temperatures in the presence of a proper combination of ceria and zirconia based electrolytes (YSZ) [8]. This behaviour has been interpreted in terms of enhanced oxygen ion transfer promoted by the doped-ceria in combination with the oxygen storage properties of YSZ [8]. It has been demonstrated by Barnett and co-workers [8] that there is a narrow temperature window (550–650 °C) in which carbon formation is not thermodynamically favoured and it is possible to utilize hydrocarbons directly [8]. Moreover, it is well known that basic oxides, MgO–CaO, are excellent supports for Ni in several heterogeneous catalytic processes [18]. Carbon deposition is prevented effectively during the reaction of CO_2 with CH_4 by supporting Ni on these supports [19]. This suppression of carbon deposition was attributed to the basicity of the MgO–CaO mixed oxides [18]. These oxides are characterised by insulating electrical properties, thus they can be used in the electronic conducting phase of SOFC electrodes only at doping levels. Barium was selected due to the high basicity characteristics of its oxide to modify the anode catalyst. It was preferred the doping of the anode catalyst surface with small amounts of Ba to avoid ohmic constraints. In the present study, the effect of barium-doping on carbon deposition during the CH_4 oxidation over a $Ni_{0.53}Cu_{0.47}$ alloy/CGO cermet catalyst has been investigated.

2. Experimental

A planar type cell architecture was used in this study. It consisted of three active layers and gold paste as a current collector for the anode and cathode.

* Corresponding author.
E-mail address: arico@itae.cnr.it (A.S. Aricò).

0378-7753/$ – see front matter © 2009 Elsevier B.V. All rights reserved.
doi:10.1016/j.jpowsour.2009.01.096

i) Anode: cermet of CGO and $Ni_{0.53}Cu_{0.47}$ alloy (50:50 wt.) (with or without barium, thickness: 15 μm)
ii) Electrolyte: CGO (20% Gd) (thickness: 300 μm)
iii) Cathode: $La_{0.6}Sr_{0.4}Fe_{0.8}Co_{0.2}O_{3-\delta}$ (thickness: 15 μm)

Synthesis of the CGO powders was done by a co-precipitation method described elsewhere [20,21]. The CGO powders were compacted by uniaxial pressing (300 MPa). The green pellet was treated at 1550 °C for 6 h in static air obtaining a disk supported electrolyte membrane (mass density, $\rho > 95\%$). The cathode electrode was deposited by spraying. The slurry was composed of a $La_{0.6}Sr_{0.4}Fe_{0.8}Co_{0.2}O_{3-\delta}$ (PRAXAIR) using isopropanol as a dispersant. The deposit was then fired at 1100 °C for 2 h under static air to ensure a good interface between electrode/electrolyte membrane. The anode was also deposited by spraying, using the same organic vehicle as for the cathode. It consisted of a gadolinia doped ceria and NiCu oxide. The anode layer was fired at 1000 °C for 2 h. The synthesis of NiCu oxide powder was done by a complexation–decomposition method described elsewhere [22]. Ba-doping was done by impregnating the calcined $NiCuO_x$/CGO mixture (50:50 wt.%) with an aqueous solution of the metal nitrate salt of Ba, followed by drying and further calcination at 773 K for 5 h. The amount of barium in the composite anode layer, as determined by X-ray fluorescence (XRF), was about 1% wt. Finally, the cell was mounted on an alumina tube, sealed with quartz adhesive (AREMCO), and heated to 800 °C in air. Reduction of the $NiCuO_x$ to a Ni–Cu alloy was carried out in situ in the presence of a hydrogen stream at 800 °C. Subsequently, the temperature was decreased to 750 °C in hydrogen. At 750 °C, time-study experiments, polarization curves and ac-impedance spectra were recorded in H_2 and CH_4 by using a Metrohm Autolab 30 potentiostat-galvanostat equipped with a FRA (frequency response analyser).

Ex-situ experiments were carried out to evaluate carbon deposition on the anode cermets during exposure to dry CH_4 and in the absence of ionic oxygen. 50 mg of a composite Ba-doped and undoped NiCu–CGO anode, previously treated at 1000 °C for 2 h in air and, subsequently, reduced at 800 °C in H_2 for 2 h, as in the cell manufacturing/conditioning procedure, were exposed to a dry methane stream at 750 °C for 100 h.

Structural analysis was done by XRD, using Bragg-Brentano (powder) or grazing angle (anode layer) configurations with a Cu Kα source operating at 40 kV and 30 mA (Philips Xpert diffractometer, Netherlands). Surface analysis was carried out by X-ray photoelectron spectroscopy (XPS) using a Physical Electronics (PHI) 5800-01 spectrometer. A monochromatic Al kα X-ray source was used at 350 W. The pressure in the analysis chamber of the spectrometer was 1×10^{-9} Torr during the measurements. To compensate for surface-charging effects, calibration of the binding energy (B.E.) scale was made with reference to the B.E. at 284.6 eV of the adventitious carbon. X-ray fluorescence analysis was done by a Bruker AXS S4 Explorer spectrometer operating at a power of 1 kW and equipped with a Rh X-ray source, a LiF 220 crystal analyzer, and a 0.128 divergence collimator.

3. Results

3.1. Physico–chemical analyses

The Ba-doped $Ni_{0.53}Cu_{0.47}O_x$/CGO cermet was studied using XRF and XPS (Fig. 1) in order to confirm the presence of barium. Table 1 shows the weight percentages of the elements contained in the anode as derived from XRF. The amount of barium was roughly 1% in the bulk. Fig. 1a shows the survey XPS spectrum of the Ba-doped $Ni_{0.53}Cu_{0.47}O_x$/CGO cermet. The peaks at 780 and 795 eV indicate a large amount of barium on the surface. Fig. 1b shows the Ba3d region in detail. Analysis of the chemical state of Ba indicates the presence of BaO. It should be pointed out that the depth of XPS analysis is typically from 3 to 5 nm. Thus, the top layers of this composite anode contain an excess of Ba-oxide. The XRD analysis of the Ba-doped cermet did not reveal the presence of a specific crystallographic Ba-phase (Fig. 2).

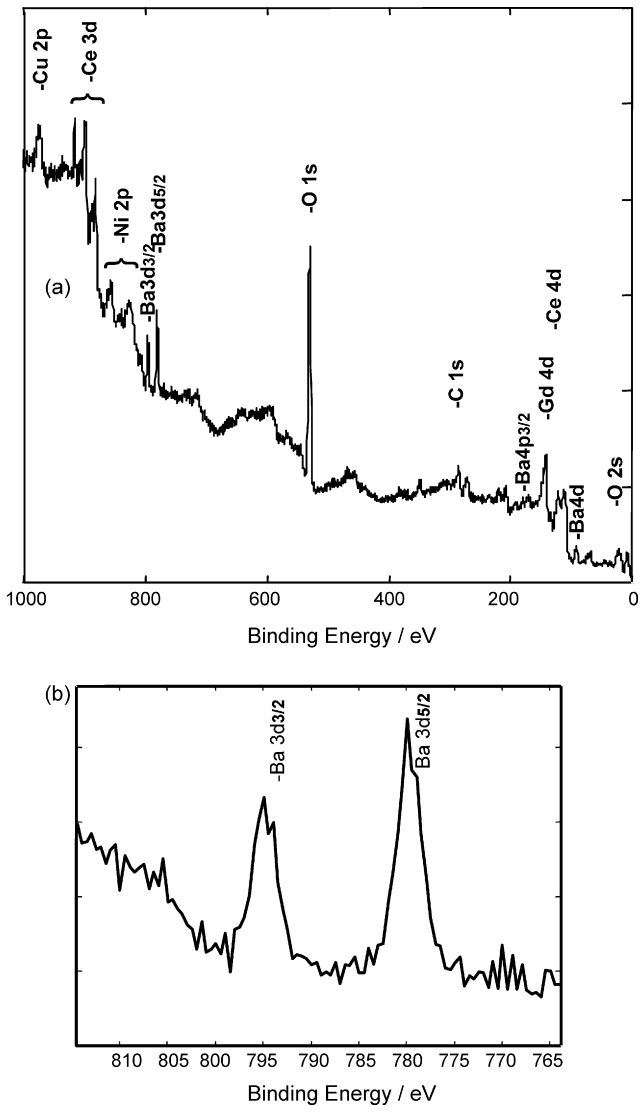

Fig. 1. (a) Survey XPS spectrum of Ba-doped $Ni_{0.53}Cu_{0.47}O_x$/CGO fresh; (b) Ba3d region in detail.

3.2. Electrochemical characterization

The anode was, in situ, reduced in hydrogen at 800 °C for 2 h to form a Ni–Cu alloy in the cermet. Cell temperature was subsequently decreased to 750 °C. Fig. 3 shows the polarization

Table 1
Weight percentages related to the elements contained in the Ba-doped $Ni_{0.53}Cu_{0.47}O_x$/CGO and in the undoped $Ni_{0.53}Cu_{0.47}O_x$/CGO. Light elements such as O and C are not detectable in this XRF analysis.

Samples	Ni (wt %)	Cu (wt%)	Ba (wt%)	Ce (wt%)	Gd (wt%)
Ba-doped $Ni_{0.53}Cu_{0.47}O_x$/CGO	27.4	25.9	1.15	39.4	5.46
$Ni_{0.53}Cu_{0.47}O_x$/CGO	28.1	27.0		38.7	6.1

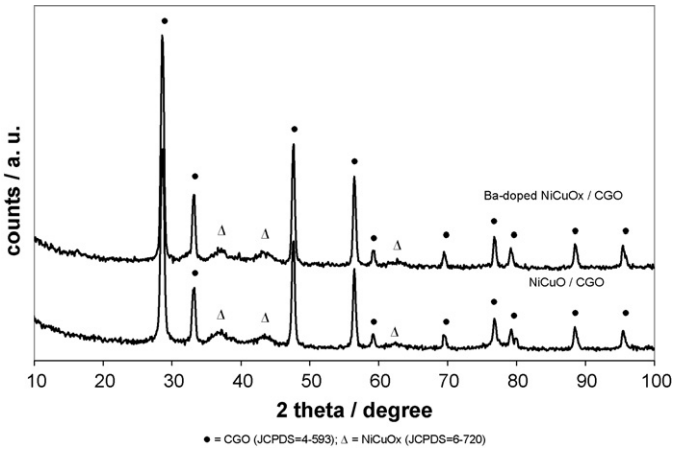

Fig. 2. Comparison of the XRD patterns of a Ba-doped $Ni_{0.53}Cu_{0.47}O_x$/CGO and undoped $Ni_{0.53}Cu_{0.47}O_x$/CGO anodes before operation in dry methane.

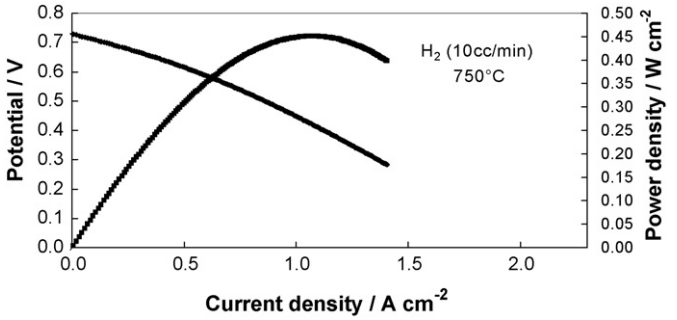

Fig. 3. Polarization and power density curves for a Ba-doped $Ni_{0.53}Cu_{0.47}$/CGO based cell fed with hydrogen at 750 °C.

curve of the Ba-doped $Ni_{0.53}Cu_{0.47}$ alloy/CGO cermet based-cell obtained in H_2 at 750 °C. The maximum power density recorded was 450 mW cm^{-2} at 0.412 V. The low open circuit voltage was due to mixed electronic-ionic conductivity of the CGO at this temperature under reducing conditions. In Fig. 4, the comparison of polarization curves and power densities is shown; these curves were obtained in dry CH_4 at 750 °C and recorded during a time-study. From the maximum power density, it is possible to observe that cell performance improves slightly from the second to the fifth day, reaching a value of 284 mW cm^{-2} at 0.7 A cm^{-2}. The improvement in electrochemical performance over time was also observed in the impedance spectroscopy (Fig. 5). The series resistance (Rs) of 0.25 Ω cm^2, registered on the second day, was close to that observed on the fifth day. This indicates that enhanced performance between the second and fifth day was not related to a decrease in

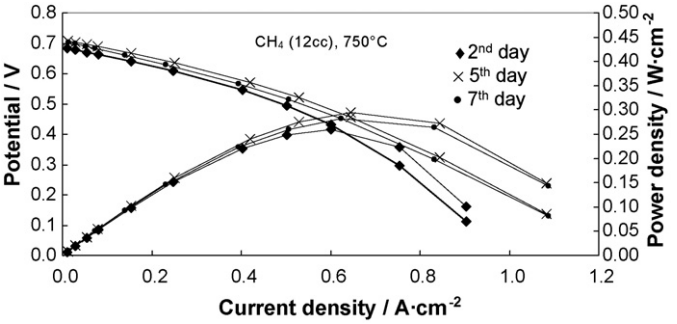

Fig. 4. Comparison of the polarization and power density curves for a Ba-doped $Ni_{0.53}Cu_{0.47}$/CGO based cell fed with methane at 750 °C and obtained at different time.

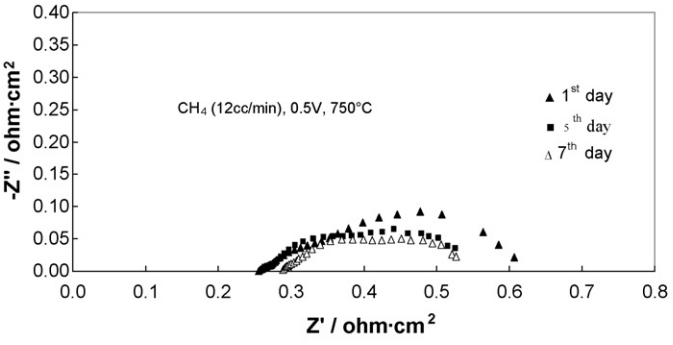

Fig. 5. AC impedance spectra for a Ba-doped $Ni_{0.53}Cu_{0.47}$/CGO based cell fed with methane at 750° and obtained at different time.

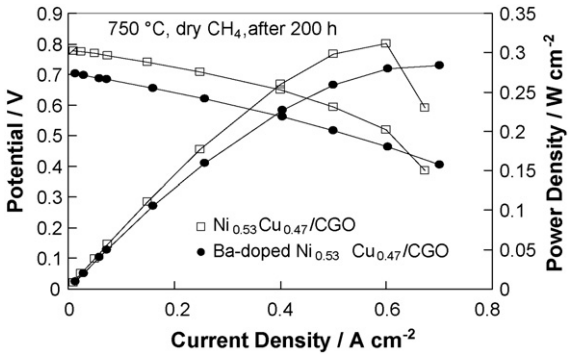

Fig. 6. Comparison of the polarization and power density curves for a Ba-doped $Ni_{0.53}Cu_{0.47}$/CGO and a $Ni_{0.53}Cu_{0.47}O$/CGO based cells fed with methane at 750 °C.

the ohmic drop. The series resistance was due mainly to the electrolyte's thickness. Polarization resistance (*R*p), instead, decreased from 0.35 to 0.27 Ω cm^2. This indicates that the electrocatalytic process improved slightly with the operation time. The electrochemical behaviour of the undoped NiCu/CGO anode as a function of time has been reported in a previous paper [5]. The increase in performance over time was more significant for the undoped anode. In the undoped anode layer, AC-impedance spectra indicated a significant decrease of series resistance over time due, possibly, to the formation of carbon fibers [5].

A comparison of polarization curves of two SOFC cells containing Ba-doped and undoped anodes at 750 °C, after 200 h tests, is reported in Fig. 6. The time-study profiles for the two anode formulations are compared in Fig. 7 at 750 °C under potentiostatic cell operation at 0.6 V. The best performance in methane was achieved by the undoped anode at 200 h. The maximum power density obtained for the $Ni_{0.53}Cu_{0.47}$/CGO based cell (310 mW cm^{-2}) was higher than that recorded for the Ba-doped $Ni_{0.53}Cu_{0.47}$/CGO

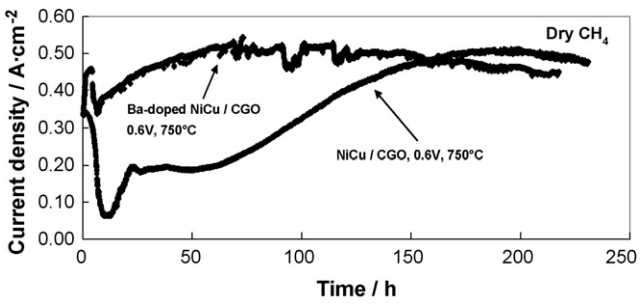

Fig. 7. Comparison of the chronoamperometric curves for a Ba-doped $Ni_{0.53}Cu_{0.47}$/CGO and a $Ni_{0.53}Cu_{0.47}O$/CGO based cells fed with dry methane at 750 °C.

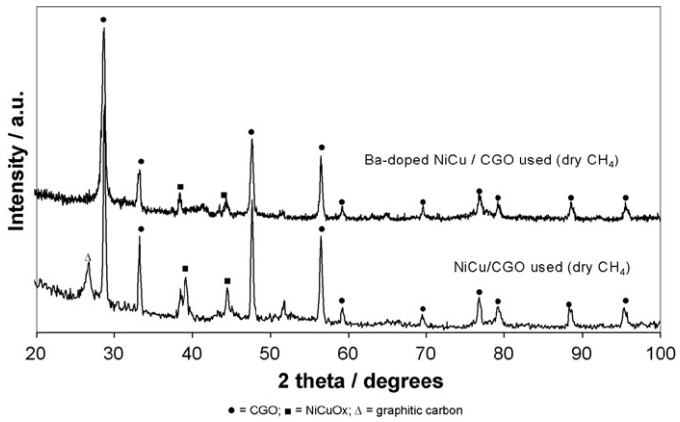

Fig. 8. Comparison of the XRD patterns of a Ba-doped $Ni_{0.53}Cu_{0.47}$/CGO and a $Ni_{0.53}Cu_{0.47}O$/CGO anodes after operation in dry methane.

(284 mW cm^{-2}). The polarization curve for both cells showed moderate potential losses as a function of time after 200 h. In the Ba-doped system, this potential decay was attributed, from ac-impedance, to an increase of series resistance (see Fig. 5, day V and VII) whereas the charge transfer resistance was essentially unaffected. Similar evidence was reported on the undoped anode [5].

3.3. Phase and chemical characterization of the anodic cermets after operation

Fig. 8 shows a comparison between XRD patterns of the anode materials after operation in dry methane for about 230 h. These patterns were obtained in the grazing angle mode (0.5° incidence angle, 1° mask) to enhance structural information from the anode layers and to reveal any trace of carbon deposition more precisely. The X-ray patterns in Fig. 8 show the presence of large intensities of CGO reflections, indicating a significant contribution from the electrolyte underlayer to the total X-ray scattering. From the XRD analysis, it can be observed that the Ba-doped $Ni_{0.53}Cu_{0.47}$/CGO anode does not show any significant carbon peak, which usually appears at 26.7° 2θ. No carbon deposition was detected by optical microscope observation of this catalyst layer. The XRD pattern of the undoped $Ni_{0.53}Cu_{0.47}$/CGO anode, instead, shows the typical peak of graphitic carbon. A splitting of the (1 1 1) reflection of the solid solution of Ni and Cu into two peaks related to Ni-rich (1 1 1) and Cu-rich (1 1 1) phases is observed in the undoped sample. This was also observed, though less evidently, in the reflection at 44.5°.

3.4. Ex-situ tests in dry methane

For a more in-depth investigation of carbon formation, 50 mg of Ba-doped and undoped anodic cermets were thermally treated in air at 1000 °C and reduced in H_2 at 800 °C, as in the cell fabrication/conditioning procedure; subsequently, they were ex-situ exposed to dry methane at 750 °C for 100 h without ionic oxygen. A comparable increase in weight was observed in both cases: 82.3 mg for the undoped catalyst and 88.5 mg for the Ba-doped catalyst. The formation of carbon fibers was also evident in both cases.

4. Discussion

As reported in the literature [23–25], the reduction of carbon deposition in heterogeneous catalysis studies of the reforming processes at Ni catalyst using K_2O, MgO, Na_2O, CaO promoters or supports can be attributed to their basicity. These oxides suppress carbon deposition during the CO_2 reforming of CH_4. The reaction kinetics observed suggest that the surface of the Ni catalyst doped with basic metal oxides is abundant in adsorbed CO_2, while the surface without them is abundant in adsorbed CH_4 [23–25]. The presence of adsorbed CO_2 on the Ni metal surface is considered an unfavorable condition for CH_4 decomposition and, as a result, carbon deposition is strongly mitigated [23].

Since carbon formation was detected in the ex-situ experiment on Ba-modified composite powder whereas it was not observed after fuel cell experiments on the same anode layer, it appears that the presence of ionic oxygen and, possibly, the use of a thin anode layer play important roles in counteracting carbon deposition in fuel cell tests. As reported in the literature [1,8], a high O^{2-} flux from the electrolyte can remove carbon from the electrode surface as it forms. However, removal of the carbon formation by O^{2-} ions is more efficient in the region near the three-phase boundary that extends no more than 10–15 μm from the electrolyte surface [26].

The carbon mechanism formation at Ni-based catalysts involves the deposition of carbon species onto the metal surface, dissolution of carbon in the bulk and, subsequently, growth of carbon fibers at the metal particles [1]. The retardation of carbon deposition in the presence of alkaline earth oxide additives is ascribed to the greater availability of (O–*) species at the metal surface due to spillover from the support [18]. The effect of alkali on carbon deposition has also been explained in terms of the stabilization of CH_x–* relative to C–* surface intermediates [27]. This retardation of carbon formation was not observed in the absence of steam [28,29]. There are several analogies between the literature on the heterogeneous catalysis at Ni supported on basic oxides and our study. In the present case, carbon deposition occurs in the ex-situ studies whereas in the fuel cell experiment, in the presence of ionic oxygen from the ceria-based electrolyte, this process is mitigated when the alkaline earth oxide is added.

XPS analysis shows that Ba is largely present on the surface of this composite layer whereas XRF revealed that Ba content in the bulk of the electrocatalyst was small. The surface chemistry in this composite anode may be similar to that of reforming catalysts based on Ni highly dispersed on MgO–CaO supports. Due to the fact that electrochemical reactions occur on the surface of electrocatalysts, surface characteristics play an important role. In steam and dry reforming processes [18,30–31], the basicity of the supporting oxide is essential for avoiding the formation of carbon deposits whereas as is well known, large carbon deposit formations occur with Ni supported on acidic oxides such as SiO_2 and Al_2O_3 [18]. However, as in the reforming catalysts, the presence of oxygen species is necessary in order to avoid the occurrence of carbon formation. By using such an approach, the surface chemistry of a supported catalyst may be reproduced in fuel cell anodes while the bulk characteristics remain, essentially, those of Ni cermets.

In addition, due to different surface characteristics of the electrocatalyst formulations, the gold paste current collector may interact in a different way with the two catalytic layers. A small infiltration of Au into the anode is not discarded. Although our experiments with only a Au-paste anode led to performances one order of magnitude lower than in the present case, an effect on the prevention of carbon deposition may not be excluded [11].

5. Conclusions

The direct utilization of dry methane in solid oxide fuel cells equipped with anodes consisting of a $Ni_{0.53}Cu_{0.47}$ alloy and gadolinia doped ceria cermets, with or without barium doping, were investigated. Similar maximum power densities of 284 mW cm^{-2} and 310 mW cm^{-2} were obtained at 750 °C for the Ba-doped $Ni_{0.53}Cu_{0.47}$/CGO and $Ni_{0.53}Cu_{0.47}$/CGO anodic cermets, respectively. As evidenced by XRD, the anode without barium showed the presence of carbon deposits whereas the anode containing barium did not show significant carbon deposits after a

200 h time-study in dry methane. Ex-situ experiments have shown that carbon formation occurs for both formulations during exposure to dry methane. This indicates that the effect of active oxygen species in depressing carbon formation is important, as demonstrated in the literature on reforming catalysts containing alkaline earth additives or basic oxide supports.

References

[1] S. McIntosh, R.J. Gorte, Chem. Rev. 104 (2004) 4845.
[2] C. Sun, U. Stimming, J. Power Sources 171 (2007) 247.
[3] P. Tsiakaras, C. Ahanasiou, G. Marnellos, M. Stoukides, J.E. ten Elshof, H.J.M. Bouwmeester, Appl. Catal. A: Gen. 169 (2) (1998) 249.
[4] A. Sin, E. Kopnin, Y. Doubitsky, A. Zaopo, A.S. Aricò, L.R. Gullo, D. La Rosa, V. Antonucci, J. Power Sources 164 (2007) 300.
[5] A. Sin, E. Kopnin, Y. Doubitsky, A. Zaopo, A.S. Aricò, L.R. Gullo, D. La Rosa, V. Antonucci, Fuel Cells 6 (2006) 137.
[6] H. Kim, C. Lu, W.L. Worrell, J.M. Vohs, R.J. Gorte, J. Electrochem. Soc. 149 (2002) A247.
[7] J.T.S. Irvine, A. Sauvet, Fuel Cells 1 (2001) 205.
[8] E. Perry Murray, T. Tsai, S.A. Barnett, Nature 400 (1999) 649.
[9] S. Tao, J.T.S. Irvine, Nature Mater. 2 (2003) 320.
[10] E.S. Putna, J. Stubenrauch, J.M. Vohs, R.J. Gorte, Langmuir 11 (1995) 4832.
[11] O.A. Marina, M. Mogensen, Appl. Catal. A 189 (1999) 117.
[12] S.-I. Lee, J.M. Vohs, R.J. Gorte, J. Electrochem. Soc. 151 (2004) A1319.
[13] C.M. Reich, A. Kaiser, J.T.S. Irvine, Fuel Cells 1 (2001) 249.
[14] A. Kaiser, J.L. Bradley, P.R. Slater, J.T.S. Irvine, Solid State Ionics 135 (2000) 519.
[15] A.T. Ashcroft, A.K. Cheetham, M.L.H. Green, P.D.F. Vernon, Nature 352 (1991) 225.
[16] A.M. Gadalla, B. Bower, Chem. Eng. Sci. 43 (1988) 3049.
[17] A.M. Gadalla, B. Bower, Chem. Eng. Sci. 44 (1989) 2825.
[18] A.P.E. York, Tian-cun Xiao, M.L.H. Green, Catal. Rev. 49 (2007) 511.
[19] O. Yamazaki, T. Nozaki, K. Omata, K. Fujimoto, Chem. Lett. 1953 (1992).
[20] J.V. Herle, T. Horita, T. Kawada, N. Sakai, H. Yokokawa, M. Dokiya, Ceram. Int. 24 (1998) 229.
[21] A. Sin, Y. Dubitsky, A. Zaopo, A.S. Aricò, L.R. Gullo, D. La Rosa, S. Siracusano, V. Antonucci, C. Oliva, O. Ballabio, Solid State Ionics 175 (2004) 361.
[22] A.S. Aricò, L.R. Gullo, D. La Rosa, S. Siracusano, A.B. Lopes Corriera Tavares, A. Sin Xicola, Solid oxide fuel cell, International Patent PCT/EP02/11963.
[23] T. Horiuchi, K. Sakuma, T. Fukui, Y. Kubo, T. Osaki, T. Mori, Appl. Catal. A: Gen. 144 (1996) 111–120.
[24] S. Albertazzi, G. Busca, E. Finocchio, R. Glockler, A. Vaccai, J. Catal. 223 (2004) 372–381.
[25] H. Morioka, Y. Shimizu, M. Sukenobu, K. Ito, E. Tanabe, T. Shishido, K. Takehira, Appl. Catal. A: Gen. 215 (2001) 11–19.
[26] M. Mogensen, S. Skaarup, Solid State Ionics 86–88 (1996) 1151.
[27] J.R. Rostrup-Nielsen, Catal. Sci. Technol. (1984); J.R. Andersen, M. Boudart (eds.); Springer: Berlin; Vol. 5, 1–117.
[28] J.R. Rostrup-Nielsen, J. Catal. 33 (1974) 184.
[29] J.L. Figueirdo, D.L. Trimm, J. Appl. Chem. Biotechnol. 28 (1978) 611.
[30] J.R. Rostrup-Nielsen, J. Catal. 85 (1984) 31.
[31] A.M. Gadalla, M.E. Sommer, J. Am. Ceram. Soc. 72 (1989) 683.